Electrochimica Acta 319 (2019) 922–932

Contents lists available at ScienceDirect

Electrochimica Acta

journal homepage: www.elsevier.com/locate/electacta

Novel sodium superionic conductor of the $Na_{1+y}Ti_2Si_yP_{3-y}O_{12}$ series for application as solid electrolyte

Adriana M. Nieto-Muñoz [a, *], Jairo F. Ortiz-Mosquera [a], Ana C.M. Rodrigues [b]

[a] Programa de Pós-graduação em Ciência e Engenharia de Materiais, Universidade Federal de São Carlos, CP 676, 13565-905, São Carlos, SP, Brazil
[b] Departamento de Engenharia de Materiais, Universidade Federal de São Carlos, CP 676, 13565-905, São Carlos, SP, Brazil

ARTICLE INFO

Article history:
Received 16 April 2019
Received in revised form
30 May 2019
Accepted 9 July 2019
Available online 10 July 2019

Keywords:
Solid electrolyte
Glass-ceramic
Sodium-ion conductor
NASICON

ABSTRACT

In the search for new materials to be used as solid electrolytes, this paper discusses the substitution of phosphorus with silicon in the $NaTi_2(PO_4)_3$ NASICON (Na-Super Ionic Conductor) compound, giving rise to the $Na_{1+y}Ti_2Si_yP_{3-y}O_{12}$ series. In fact, the substitution of P^{+5} for Si^{+4} enables the increase in the Na^+ charger carrier concentration. The solid electrolytes are synthetized by the glass-ceramic route, which consists in the controlled crystallization of a precursor glass subjected to specific heat treatment. Experimental results indicate that precursor glasses are successfully crystallized in compositions containing $y \leq 1.2$. X-ray diffraction patterns show the formation of NASICON phase in the $Na_{1+y}Ti_2Si_yP_{3-y}O_{12}$ glass-ceramics for $y \leq 0.8$. However, with further addition of silicon, the major crystalline phase obtained is the $Na(TiO)(PO_4)$ phase. Surprisingly, the electrical characterization reveals that the $y = 1.0$ sample, whose main phase is the non-NASICON $Na(TiO)(PO_4)$, exhibits the lowest activation energy (0.31 eV) and the highest ionic conductivity of 1.0×10^{-4} S cm^{-1} at room temperature and 1.7×10^{-2} S cm^{-1} at 300 °C. Rietveld refinement and electrical conductivity results suggest that the increased ionic conductivity in the $Na(TiO)(PO_4)$ phase is due to the inclusion of some Si^{+4} ions in its structure, thus forming a new and highly $Na(TiO)((Si)PO_4)$ conductive phase.

1. Introduction

Environmental problems and the depletion of natural resources are among the main reasons for increasing interest in the search for new, alternative, cheap, eco-friendly energy sources [1–3]. Over the past decade, lithium ion batteries (LIBs) have become the market leader for energy storage in portable devices due to the highly attractive combination of lithium-ion properties, such as: a) the very negative redox potential, and hence, high voltage of lithium-based cells, b) low atomic weight, which allows for devices of high volumetric energy density, and c) small ionic radius, enabling its rapid diffusion into solids, which is a significant advantage in the development of all solid-state devices. However, the use of lithium in stationary energy storage devices is unfeasible, given the high extraction costs and the limited accessibility to this element, whose deposits are frequently located in environmentally protected areas [3–5]. In this context, several studies in recent years have reported that alkali metal sodium-based batteries constitute an excellent alternative for energy storage. Because sodium is a widely available chemical element, its production and extraction are inexpensive. Moreover, the toxicity of sodium is low, and its electrochemical redox potential is similar to that of lithium. These characteristics make this element a promising option for the development of future energy storage devices [5–8].

The two most readily available types of sodium ion batteries on the market today are ZEBRA and Na/S [9]. However, despite their use in electric cars and other devices, they present problems such as flammability and corrosivity, which, combined with high operating temperatures, cause degradation of the cell components. One of the most feasible ways to solve these problems is to optimize the solid electrolyte properties, thereby lowering the working temperature of sodium batteries [3,10–12]. Many solid materials are known to be sodium conductors. One of the most promising and interesting solid materials are those belonging to the NASICON (**Na**-Sodium **S**uper **I**onic **C**onductor) family. The high ionic conductivity exhibited by these materials (between 10^{-4} and 10^{-2} S cm^{-1} at room temperature [9,13,14]), as well as their ready acceptance of different ions in their structure, leading to solid solutions with enhanced ionic conductivity, has generated great interest in their

* Corresponding author.
E-mail address: adriana.nieto@ppgcem.ufscar.br (A.M. Nieto-Muñoz).

https://doi.org/10.1016/j.electacta.2019.07.032
0013-4686/

use as solid electrolytes in sodium-ion batteries. The molecular formula of these materials is $A_xM_2(XO_4)_3$, where A is usually a monovalent cation (Na^+, Li^+, K^+), M is a tetravalent cation such us Ti^{+4}, Ge^{+4}, or Sn^{+4}, and X may be P^{+5} or Si^{+4} [9,15–17]. The NASICON structure can be described as an arrangement of MO_6 octahedra linked by corners to XO_4 tetrahedra that produce a three-dimensional $M_2(XO_4)_3$ arrangement with channels through which A ions can move very easily, leading to very high ionic conductivities in the case of some specific compositions with low activation energy [6,18,19]. The wide range of compositional variations of the NASICON family allows for partial or total replacement of the A, M or Si^{+4}/P^{+5} ions, making them interesting materials for investigations about the influence of different elements in their ionic conductivity [9,20].

The various NASICON materials described in the literature include the $NaTi_2(PO_4)_3$ (NTP) compound and related solid solutions. Few descriptions are available of the substitution of P^{5+} with Si^{4+} in this system. In fact, Tsuji et al. [21] synthesized materials of this system by solid state reaction, substituting phosphorus ions with silicon ions to form the $Na_{1+y}Ti_2Si_yP_{3-y}O_{12}$ (NTSP) series. The authors made substitutions of $y = 0.0$, 1.0 and 1.5. However, they only succeeded in obtaining a single phase NASICON type compound in the sample without silicon (NTP). In addition, these authors reported that X-ray diffraction (XRD) patterns of their NTSP materials with $y = 1.0$ and 1.5 revealed, together with the NASICON crystalline phase, the presence of TiO_2 and SiO_2. Kishioka et al. [22], in turn, synthesized glass-ceramics from parent glasses with $3Na_2O{\cdot}67TiO_2{\cdot}30P_2O_5$ and $3Na_2O{\cdot}72TiO_2{\cdot}25P_2O_5$ compositions and a content of 5 mol % of SiO_2. The precursor glasses were crystallized in a single-step heat treatment of 30 h at temperatures varying from 800 to 1000 °C. XRD patterns revealed the formation of the NASICON phase in both compositions after the heat treatments. Kishioka et al. also suggested the formation of a solid solution with the inclusion of silicon ion (Si^{+4}) in the NTP system. These authors also found peaks of secondary phases such as TiO_2, TiP_2O_7, and $(TiO)_2P_2O_7$. Tsuji et al. and Kishioka et al. obtained the NASICON phase but provided no data on the ionic conductivity of these interesting materials.

In our search for possible candidates for solid electrolytes that are conductive by sodium ions, we synthesized and optimized the $NaTi_2(PO_4)_3$ (NTP) NASICON system via the glass-ceramic route. Many authors have shown that one of the advantages of the glass-ceramic route over classical methods of ceramic processing is that it reduces the final porosity and allows for microstructural control by suitable thermal treatments, which can contribute for improving the ionic conductivity of the material [14,20,23]. On the other hand, it is known that the inclusion of aliovalent ions of lower valences than those ions who forms the NASICON skeleton structure, i. e, in our case, P^{5+} and Ti^{4+} ions, can enhance its conductivity, because the introduction of those ions generates an excess of negative charge that must be compensated by increasing the number of sodium ions, which means an increase in the concentration of charge carriers, and thus, in the ionic conductivity. In this context, to improve the ionic conductivity of the NTP material, silica was added to substitute P^{+5} ions with Si^{+4} ions, thus forming the $Na_{1+y}Ti_2Si_yP_{3-y}O_{12}$ (NTSP) series. In this work, precursor glasses of $Na_{1+y}Ti_2Si_yP_{3-y}O_{12}$ ($0.0 \leq y \leq 3.0$) composition were obtained in the compositional range of $y = 0.0$ to 3.0 and characterized by thermal analysis. Glass-ceramics were obtained by single thermal treatment at their respective crystallization temperature. XRD and Rietveld refinement revealed that the NASICON phase was obtained as major phase in the glass-ceramics up to the $y = 0.8$ composition. However, the $Na(TiO)(PO_4)$ crystalline compound was observed as major phase in compositions with higher silicon contents, $y = 1.0$ and 1.2. Impedance spectroscopy results indicate that the ionic conductivity of the samples containing NASICON phase increased by up to four orders of magnitude in response to the addition of silicon when compared with the original silicon-free NTP system. Surprisingly, in this work, the highest ionic conductivity was achieved by the NTSP10 ($y = 1.0$) sample, in which the non-NASICON $Na(TiO)(PO_4)$ crystalline compound was the major crystalline phase. Lastly, the glass-ceramics microstructures revealed by scanning electron microscopy (SEM) are also discussed in light of their different silicon contents.

2. Experimental methods

2.1. Synthesis of precursor glasses

The parent glasses of NTSP glass-ceramics were obtained in batches of 20 g by the conventional melt quenching method. This method consists of melting the precursor raw materials and then cooling the resulting liquid. To increase the cooling rate, the liquid was splat-cooled, i.e., pressed between two metal plates, resulting in a vitreous material. Stoichiometric amounts of sodium carbonate (Na_2CO_3, Vetec 99.9%), titanium dioxide (TiO_2, Aldrich > 99.9%), dihydroxy ammonium phosphate ($(NH_4)_2HPO_4$, Aldrich > 98%) and silica dioxide (SiO_2, Zetasil2 > 99%) were used as starting materials. The powders were homogenized in a rotary ball mill with alumina balls for 12 h, after which they were placed in a platinum crucible and heated for 6 h to temperatures ranging from 400 to 700 °C to remove volatile compounds (CO_2, NH_3, H_2O) from the Na_2CO_3 and $(NH_4)_2HPO_4$ raw materials. The mixture was then heated to temperatures of 1400–1500 °C for 30 min. The different precursor glasses were annealed at a temperature below their glass transition temperature (T_g) (thermal characterization given below), i.e., T_g - 40 °C, for 2 h to relieve possible thermal stresses.

2.2. Glass characterization, crystallization of precursor glasses, and glass-ceramics characterization

The characteristic temperatures of precursor glasses, such as glass transition temperature (T_g) and crystallization temperature (T_x), were determined by differential scanning calorimetry (DSC) using platinum crucibles in an air atmosphere and applying a heating rate of 10 °C/min in a temperature range of 30–1000 °C.

To obtain NTSP glass-ceramics, small pieces of each precursor glass were subjected to single-step heat treatments carried out at the onset of the DSC crystallization peak (Table 1) for 30 min. In a single-step heat treatment, the nuclei generated during the glass synthesis, or more precisely, during the cooling of the liquid glass, grow to the size of crystals. These heat treatments were performed in a tubular electric furnace with temperature control and stability of ±1 °C.

The amorphous nature of the glass samples and the crystalline phases of the NTSP glass-ceramics were respectively confirmed and determined by XRD, using a Rigaku Ultima IV X-ray diffractometer with Cu K_α radiation, operating in the 2θ range of 10°–80° with an integration time of 0.6 s and a scan step size of 0.02°. In some cases, the XRD procedure was performed with a 0.02° step size and 0.1 s integration time to allow for refinement of the crystal structures. The crystalline phases were identified using the Crystallographica Search-Match software [24], and the Rietveld analysis was performed using Topas-Academic version 6 [25] with crystallographic information framework (CIF) files from the Inorganic Crystal Structure Database (ICSD) [26].

For the electrical conductivity measurements, the glass-ceramic samples were sanded to ensure flat parallel surfaces. Gold electrodes were then sputtered on both surfaces. Electrical measurements were taken by impedance spectroscopy at temperatures of

50–300 °C, in the frequency range of 1 MHz to 0.01 Hz, using a Novocontrol Alpha Analyzer – a high-performance frequency analyzer, coupled to a Novotherm furnace whose temperature is adjustable with a precision of ±0.1 °C. The WinFit software was used for data acquisition.

The glass-ceramic microstructures were examined on the fracture surfaces of sample using a scanning electron microscope (SEM) equipped with an EDS (energy dispersive spectroscopy) detector with a beam voltage of 10–25 kV.

3. Results and discussion

3.1. Differential scanning calorimetry

Table 1 summarizes the nominal composition and the characteristic temperatures (T_g and T_x) of the NTSP parent glasses, while Fig. 1-a shows the DSC thermograms of some of the precursor glasses. Thermograms in Fig. 1-a show the presence of an endothermic event, corresponding to the glass transition temperature, followed by an exothermic peak which corresponds to the glass crystallization. The crystallization temperature (T_x) was taken as the onset of the crystallization peak. It is worth noting that the intensity of the crystallization peak decreases with increasing y, becomes very low for sample with $y = 2.5$ (NTSP25), while in the $y = 3.0$ (NTSP30) sample, this peak is barely visible.

The thermograms in Fig. 1-a also show a small peak in the endothermic direction after the crystallization peak. All the parent glasses of the NTSP system showed this small peak around 850 °C, which cannot be ascribed to the final melting temperature that varied around 1400–1500 °C, according to our experimental melting conditions. During our heat-treatments experiments, it was found that vitreous samples heated close to 850 °C were bonded to the crucible. This may be attributed to the onset of melting of the crystalline phase. In fact, similar endothermic peaks were observed in thermograms of both $Li_2O{\cdot}SiO_2 - CaO{\cdot}SiO_2$ [27] and $Na_2O{\cdot}2CaO{\cdot}3SiO_2$ glasses [28]. The authors explained that the beginning of this endothermic peak corresponds to the solidus temperature of the phase diagram, in which the first liquid of the melting appears.

A silica-free NTP glass could not be obtained, probably because of the high percentage of titanium oxide (TiO_2), which is not a glass-former (see Table 1). Therefore, the characteristic glass transition (T_g) and crystallization (T_x) temperatures could not be determined, since the melted material devitrified during its cooling process. However, conductivity measurements and structural characterization of the crystallized NTP samples were taken to underpin the discussion about the effects of adding silicon to NTSP glass-ceramics.

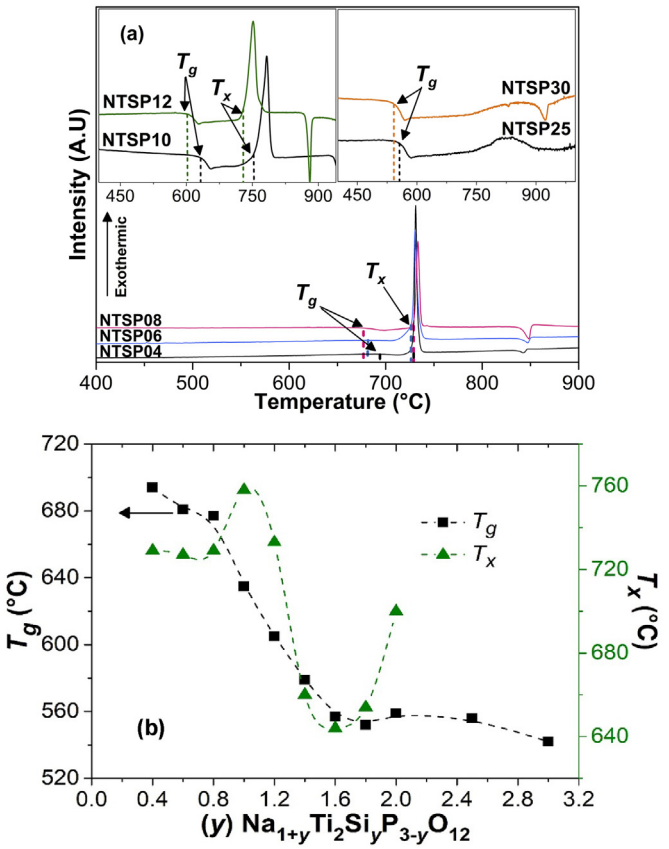

Fig. 1. (a) DSC thermograms of NTSP ($Na_{1+y}Ti_2Si_yP_{3-y}O_{12}$) precursor glasses obtained at a heating rate of 10 °C.min^{-1} and (b) evolution of glass transition temperature (T_g) and crystallization temperature (T_x) as a function of silicon content (y). The lines in the figure are drawn to guide the eyes. Error bars are smaller than the data symbols. (For interpretation of the references to colour in this figure legend, the reader is referred to the Web version of this article.)

Fig. 1-b shows the influence of silica content on the characteristic temperatures of NTSP glasses. As can be seen, the glass transition temperature (T_g) decreased as P^{+5} were partially replaced by Si^{+4} cations. It should be noted that the addition of silicon, in turn, was accompanied by the inclusion of sodium ions in the NTSP system (see Table 1). In this regard, the decrease in T_g values may be

Table 1
Nominal composition (mol %) and characteristic temperatures of $Na_{1+y}Ti_2Si_yP_{3-y}O_3$ (NTSP) precursor glasses. T_g = glass transition temperature, T_x = crystallization temperature measured at the onset of the crystallization peak.

Sample name	y	Na_2O	TiO_2	SiO_2	P_2O_5	T_g (°C) (±2 °C)	T_x (°C) (±2 °C)
		(mol %)					
NTP (without Si)	0.0	12.5	50.0	–	37.5	–[a]	–[a]
NTSP04	0.4	15.9	45.5	9.1	29.5	694	729
NTSP06	0.6	17.4	43.5	13.0	26.1	681	727
NTSP08	0.8	18.8	41.7	16.7	22.9	677	729
NTSP10	1.0	20.0	40.0	20.0	20.0	635	758
NTSP12	1.2	21.2	38.5	23.1	17.3	605	733
NTSP14	1.4	22.2	37.0	25.9	14.8	579	660
NTSP16	1.6	23.2	35.7	28.6	12.5	557	644
NTSP18	1.8	24.1	34.5	31.0	10.3	552	654
NTSP20	2.0	25.0	33.3	33.3	8.3	559	700
NTSP25	2.5	26.9	30.8	38.5	3.8	556	–
NTSP30	3.0	28.6	28.6	42.9	–	542	–

[a] Did not form glass: devitrified during cooling.

attributed to an increase in the number of non-bridging oxygen atoms in the glass structure resulting from the introduction of the Na_2O modifier.

No noticeable change in crystallization temperature (T_x) was visible in the first three compositions. However, the T_x of the NTSP08 sample increased, followed by a constant decrease up to $y = 1.6$, which showed a minimum value of T_x. The behavior of T_x around $y = 1.0$ will be explained by the emergence of different crystalline phases in these glass-ceramics, as will be discussed in section 3.2.

3.2. X-ray diffraction (XRD)

Fig. 2 shows the XRD patterns of the glass samples of compositions $y = 0.6$ (NTSP06), $y = 1.2$ (NTSP12) and $y = 3.0$ (NTSP30) obtained after the melting process. Results similar to those depicted in Fig. 2 were obtained for all the other parent glasses. The formation of a characteristic amorphous halo is evidenced in the range of $15° < 2\theta < 40°$, which shifts to higher angles in response to increased silicon content. Note the absence of diffraction peaks that would indicate the formation of crystalline phases. This confirms that all the NTSP compositions under investigation were successfully vitrified.

Fig. 3-a shows the XRD patterns of glass-ceramics obtained by the crystallization of precursor glasses heat treated at their respective T_x (see Table 1) for 30 min. These patterns indicate that the heat treatments applied to the glass compositions containing $y \leq 0.8$ led to the formation of the NASICON crystalline phase (ICSD 1530649) as the major phase. However, the pattern of the NTSP06 sample also reveal some traces of crystalline phases such as $Na_4(TiO)(PO_4)_2$ (ICSD 74566) and TiO_2 (ICSD 9009086) which are indicative of a limit of the NASICON solid solution. This also suggests that the precursor glasses of composition $y \geq 0.6$ are non-stoichiometric, i.e., there are no crystals with identical composition to that of the parent glass. The NTSP08 sample shows peaks of the same crystalline phases as the NTSP06 sample, plus a small amount of $Na(TiO)(PO_4)$ (ICSD 1535856) phase. An amorphous halo around $2\theta = 25°$ in compositions containing $y > 1.4$ is present, indicating that a residual glassy phase still remains. This suggests that the heat treatments applied to those compositions did not crystallize the material completely. On the other hand, the absence of crystallization peak in DSC thermograms (Fig. 1-a) of parent glasses with higher silicon content ($y = 2.5$ and 3.0) indicate that those glasses cannot crystallize under heat treatment conditions.

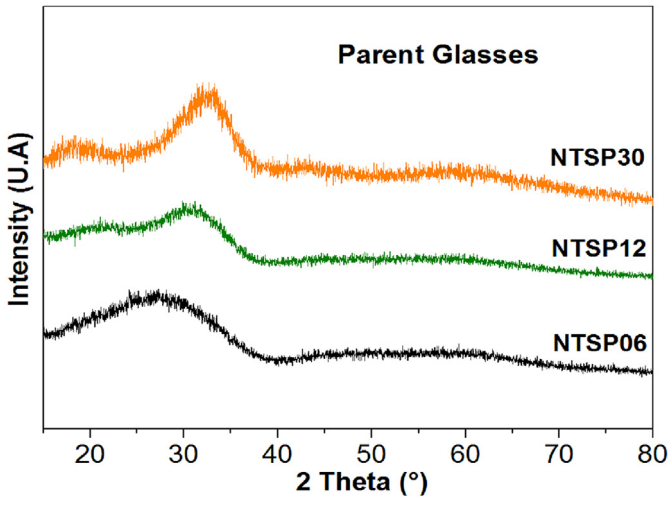

Fig. 2. XRD patterns for NTSP06 ($y = 0.6$), NTSP12 ($y = 1.2$) and NTSP30 ($y = 3.0$) precursor glasses of the $Na_{1+y}Ti_2Si_yP_{3-y}O_{12}$ system.

Since the content of $Na(TiO)(PO_4)$ phase gains greater importance as the silica content (y) increases, with significant effects on the total ionic conductivity, as discussed later in the 3.4 section, it was necessary to quantify the main phases in the NTSP compounds by the Rietveld refinement method. The results of percentages of crystalline phases are depicted in Fig. 4-a.

From Fig. 4-a, it is evident that the amount of NASICON phase in the NTSP system decreases with the addition of silicon, dropping to 5.5% and 2.4% in the $y = 1.0$ and 1.2 samples, respectively. Thus, the $Na(TiO)(PO_4)$ (NTPO) compound becomes the major crystalline phase in the NTSP10 and NTSP12 compositions. The development of this new phase can be corroborated by the sudden rise in crystallization temperature, as illustrated in Fig. 1-b for composition $y = 1.0$, since a different T_x would be required for the formation of this non-NASICON phase.

The NTPO compound belongs to the titanyl phosphate family: $M(TiO)(PO_4)$, where M = K, Na, Rb, Tl, Ag or NH_4 [29]. The crystalline structure of these materials is very similar to the NASICON structure, since it is also composed of TiO_6 octahedra and PO_4 tetrahedra that share corners. However, one of the differences with the NASICON structure is the asymmetry exhibited by TiO_6 octahedra in the $M(TiO)(PO_4)$ family. As Tordjman et al. [30] demonstrated, the distances between titanium and oxygen differ within the TiO_6 octahedron, i.e., some are shorter than others, causing a distortion in the direction of the c axis of the unit cell. According to some authors, the nonlinear optical properties and one-dimensional ionic conductivity exhibited by these materials are partly due to this distortion [31,32].

For further discussion about the glass-ceramic microstructure (section 3.3), it should be noted that the diffractograms of NTSP glass-ceramics (Fig. 3-a) show no peaks associated with crystalline SiO_2, or with any compound containing silica. The only exception is the NTSP10 composition, since the Rietveld analysis (Fig. 3-b) showed a very small peak attributed to SiO_2.

Fig. 4-b shows the evolution of the lattice parameters in the NASICON structure as the amount of silicon in the precursor material increases. In view of the evident increase in both parameters a and c (Table 2), the data obtained confirm the inclusion of silicon in place of phosphorus in the NASICON crystalline structure up to $y = 0.8$. This increase in the lattice parameters, which in turn causes the cell expansion of the NASICON structure, can be explained by the larger size of the Si^{+4} ions (0.26 Å) compared to the ionic radius of P^{+5} phosphorus (0.17 Å) [33]. These results are in good agreement with those of similar studies in which phosphorus was replaced by silicon in some NASICON materials of different chemical compositions. In fact, Shimadzu et al. [34], who synthesized NASICON ceramics with the molecular formula $Na_{1+x}Zr_2Si_xP_{3-x}O_{12}$ by solid-state reaction, reported that the inclusion of silicon increases the lattice parameters and the unit cell volume due to the formation of larger $[SiO_4]^{-4}$ tetrahedra as compared to $[PO_4]^{-3}$ tetrahedra. Yadav et al. [35] also reported an increase in the unit cell volume as a consequence of Si^{4+}/P^{5+} substitution, for samples of the same composition as those studied by Shimadzu et al. but produced by the sol-gel method.

The shrinkage of unit cells in glass-ceramics samples with compositions of $y \geq 1.0$ (Fig. 4-b) is attributed to the formation of $Na(TiO)(PO_4)$ crystalline phase. In this context, the added silicon ions appear to preferentially substitute phosphorus ions in the NTPO structure but not in the NASICON structure. The results of the Rietveld analysis (not shown in this paper) indicate that the NASICON phase was absent from compositions with $y > 1.4$.

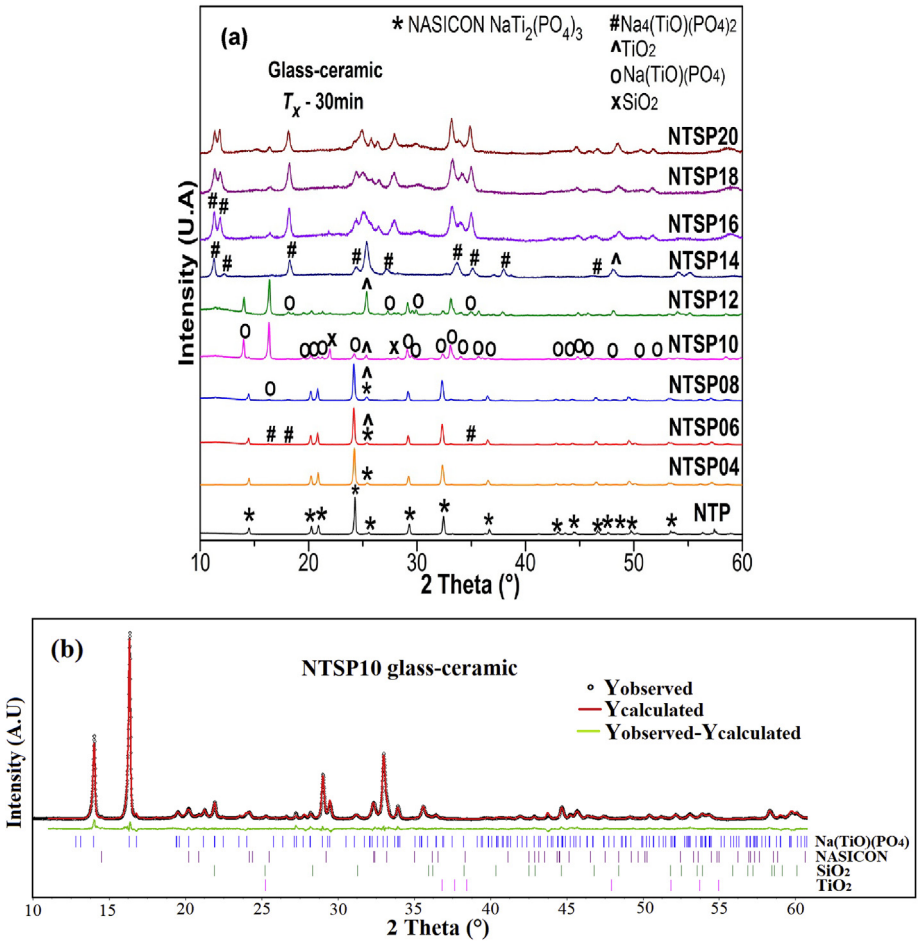

Fig. 3. (a) XRD patterns of NTSP glass-ceramics obtained after heat treatment of the parent glasses at their corresponding crystallization temperature (Table 1) for 30 min. (b) Rietveld refinement of XRD data of the NTSP10 glass-ceramic with R-factors: $R_{wp} = 10.91\%$ and $R_p = 7.98\%$.

3.3. *Scanning electron microscopy (SEM)*

Fig. 5 illustrates the microstructure and crystal morphology of the NTSP glass-ceramics with compositions containing $y = 0.4$ (NTSP04) to $y = 1.8$ (NTSP18). In general, these SEM micrographs depict glass-ceramics with poorly defined grains. The different microstructures also reveal the formation of spherical particles (except for composition NTSP04, Fig. 5a) whose main size increases along with increasing silicon content, up to NTSP14, Fig. 5f.

In order to identify the elements in the spherical particles ("ball") and in the matrix ("matrix"), the glass-ceramic samples NTSP08 and NTSP10 were subjected to a microanalysis by energy dispersive X-ray spectroscopy (EDS). The results obtained are shown in Fig. 6(a–d). The data garnered from the EDS analysis indicate that the chemical composition of the grains ("balls") and matrix of the NTSP08 and NTSP10 glass-ceramics consisted of the same elements, since all the EDS graphs showed peaks associated with Ti, P, O, Na and Si elements. However, it should be mentioned that the proportion or quantity of each element differed. In this regard, it is estimated that the "balls" had higher silicon and oxygen contents than the matrix in which they are dispersed. These results suggest that the spherical particles in the samples are composed of silica. However, because the XRD patterns of the NTSP glass-ceramics did not show peaks associated with crystalline SiO_2 except in the NTSP10 sample, it can be deduced that the nature of the silica is non-crystalline.

In order to identify the origin of these silica "balls" in the NTSP glass-ceramics, SEM micrographs of the fractured surface of the NTSP10 precursor glass were also recorded as shown in Fig. 6(e and f).

As can be seen in Fig. 6-e, the precursor glass also contained spherical particles before any heat treatment was applied. These aggregates consist mainly of silica and oxygen, according to the EDS analysis (see Fig. 6-f), indicating that non crystalline silica was formed in the glass synthesis, during the cooling of the melt, which underwent liquid-liquid phase separation. This type of microstructure was also identified by Oliveira et al. [36] in glasses containing SiO_2 and P_2O_5. These authors stated that vitreous silica particles are formed in the glass forming process, as the liquid cools, because a constant decrease in the temperature increases the viscosity of silica, thus preventing it from diffusing through the liquid. This finding is relevant in the context of our research, since it suggests that part of the added silicon does not substitute the phosphorus in the investigated glass-ceramics.

This suggests that the silica particles revealed in the glass-ceramics of Fig. 5 were generated as the glass was synthesized, i.e., before it crystallized. The increase in size of these silica particles is ascribed to a greater tendency for liquid-liquid phase separation in the precursor glasses in which the P_2O_5 content is higher or similar to that of SiO_2. However, in the $y \geq 1.6$ composition, the SiO_2 content exceeds that of P_2O_5, causing the glass to behave like a silicate glass and thus diminishing the tendency for liquid-liquid

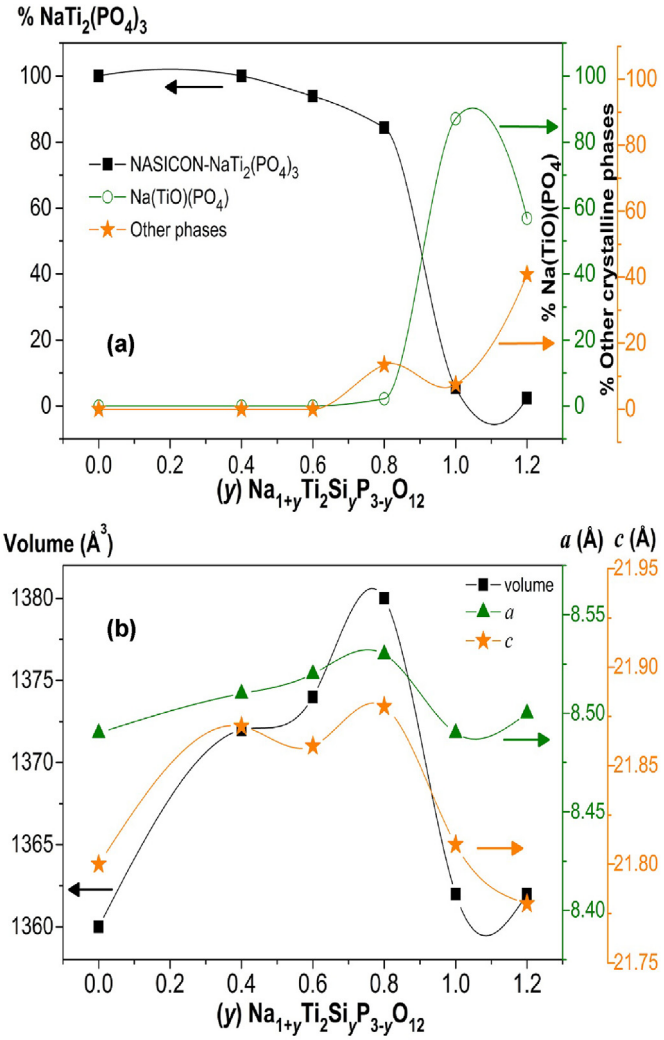

Fig. 4. (a) Quantity (weight percent, %) of crystalline phases, and (b) evolution of the lattice parameters of the $Na_{1+y}Ti_2Si_yP_{3-y}O_{12}$ NASICON structure as a function of silicon content (y). The line between symbols is a guide for the eye. Uncertainty values are smaller than the symbol size. (For interpretation of the references to colour in this figure legend, the reader is referred to the Web version of this article.)

Table 2
Lattice parameters of the NASICON structure and R-factors (R_{wp} and R_p) from Rietveld analysis of NTSP glass-ceramics obtained by heat treatment at corresponding T_x (see Table 1) for 30 min.

Sample	a (Å)	c (Å)	V (Å^3)	R_{wp} (%)	R_p (%)
NTP (without Si)	8.49	21.80	1360	21.20	15.76
NTSP04	8.51	21.87	1372	14.30	10.12
NTSP06	8.52	21.86	1374	9.08	6.34
NTSP08	8.53	21.88	1380	10.64	7.92
NTSP10	8.49	21.81	1362	10.91	7.97
NTSP12	8.50	21.78	1362	10.31	8.06

phase separation.

3.4. Complex impedance spectroscopy and ionic conductivity

Fig. 7-a shows complex impedance plots, i.e., the so-called Nyquist diagram, of different NTSP glass-ceramics recorded at 50 °C. Only results of compositions $y = 0.4$ (NTSP04) to 1.2 (NTSP12) are presented since the heat treatments performed on the samples with higher silica content ($y > 1.4$) did not lead to their complete crystallization, as indicated by the XRD patterns in Fig. 3-a. For this reason, these samples were not subjected to electrical characterization.

The Nyquist diagram of NTSP glass-ceramics (Fig. 7-a) shows two different responses. The first is a semicircle formed in the region of high and medium frequencies, which is associated with the intrinsic material response. The second phenomenon is the sloped line in the low-frequency region, which represents the blocking of ions at the electrode-sample interface. This straight line is characteristic of ionic conductive materials. As can be seen in the complex impedance plots, the grain and grain boundary response could not be identified because of the presence of a single semicircle. On the other hand, the total resistivity of the samples can be read at the intersection of the semicircle with the real axis in the low-frequency region. Also, increasing the amount of silicon in the NTSP system causes a decrease in the total resistivity of compositions up to $y = 1.0$ (NTSP10). However, the (NTSP12) composition clearly showed an increase in the resistivity value. All the Nyquist plots recorded in the 50–300 °C temperature range showed a similar format. The real (Z') and imaginary (Z'') parts of impedance were divided by the geometric factor (L/A, L being the sample thickness, and A the area in contact with the gold electrodes). Thus, sample resistivity (ρ_{TOTAL}) is read at the low frequency intersection of the semi-circle to the x axis. The total ionic conductivities (σ_{TOTAL}) of the NTSP glass-ceramics were thus calculated by applying $\sigma_{TOTAL} = 1/\rho_{TOTAL}$. The total ionic conductivities were then plotted (Fig. 7-b) according to an Arrhenius equation:

$$\sigma_{TOTAL} = \sigma_o \exp(-E_a/k_B T) \quad (1)$$

where E_a is the activation energy for ionic conduction, σ_o is the pre-exponential factor, and T and k_B are the absolute temperature and Boltzmann constant, respectively.

The activation energy (E_a), the logarithm of the pre-exponential factor (log σ_0), and the total conductivity at 300 °C, ($\sigma_{300°C}$) were determined from the linear regression of data in Fig. 7-b and shown in Table 3.

As can be seen in Fig. 7-c, the inclusion of silicon leads to a considerable decrease in the activation energy when compared to that of the glass-ceramic produced without silicon ($y = 0.0$ or NTP). In addition, the values of the logarithm of the pre-exponential term of the Arrhenius equation presented in Table 3, except for the NTP sample, are in good agreement with those reported in the literature for lithium and sodium-conductive NASICON glass-ceramics which range from 0.2 to 2.0 [14,15]. Thus, the increase in the total ionic conductivity by up to five orders of magnitude is attributed to the decrease in the activation energy.

Since the NASICON phase is the major crystalline phase in the samples whose compositions contain up to $y = 0.8$, the increase in total conductivity in this range of y is attributed not only to the increase in the sodium ion concentration but also to the expansion of the NASICON unit cell in response to the introduction of larger Si^{4+} cations than P^{5+} cations, as discussed in Section 3.2 (see Fig. 4-b). This increase in volume presumably enables sodium ions to move more easily in the NASICON crystal structure, which is reflected in the decrease in activation energy.

On the other hand, the high ionic conductivity of NTSP10 and NTSP12 samples was unexpected, in view of the formation of $Na(TiO)(PO_4)$ phase as the major crystalline phase instead of the NASICON phase. As can be seen in Fig. 7-c and Table 3, the ionic conductivity of the NTSP10 glass-ceramic was one order of magnitude higher than that of the samples whose major crystalline phase was NASICON.

The $Na(TiO)PO_4$ crystalline phase present in the NTSP10 and

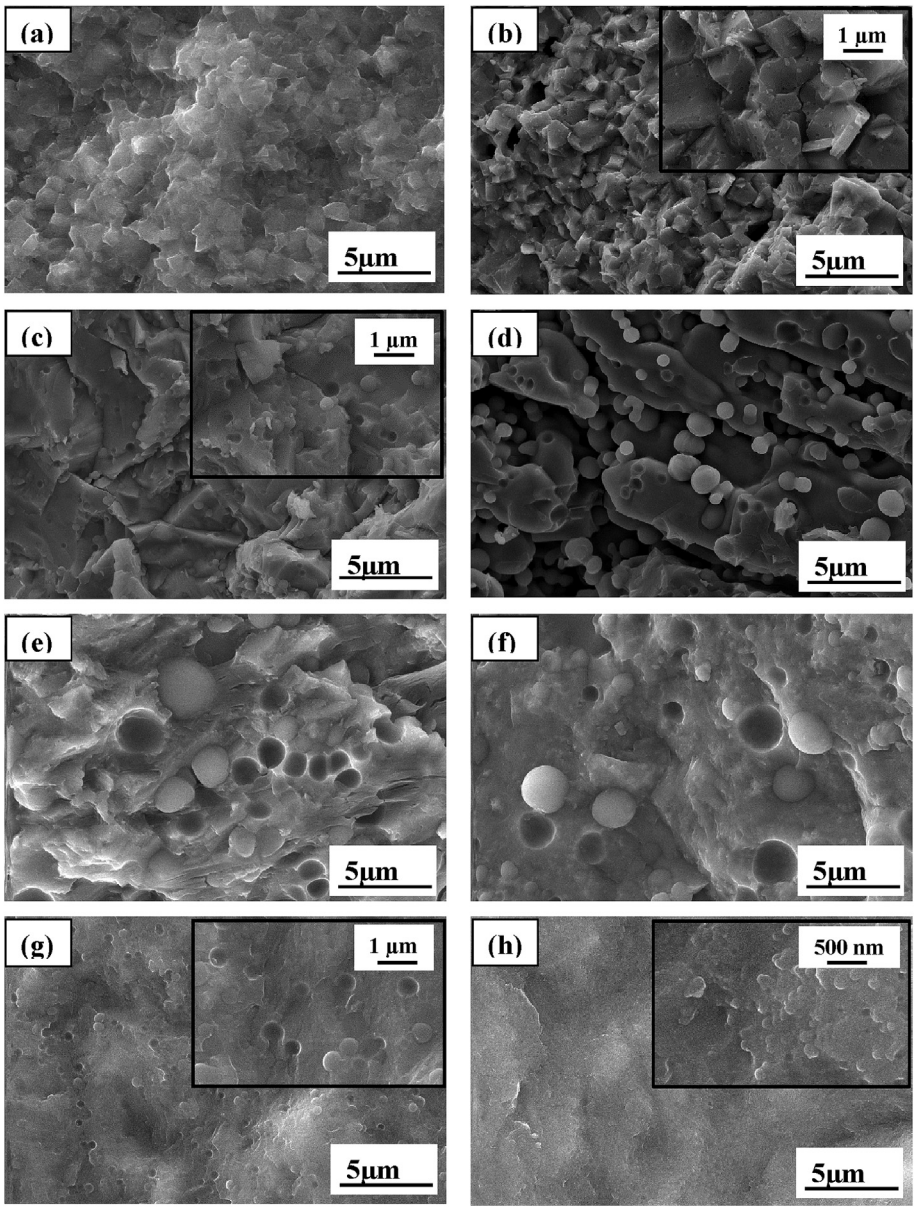

Fig. 5. Microstructures of the fracture surfaces of $Na_{1+y}Ti_2Si_yP_{3-y}O_{12}$ (NTSP) glass-ceramics obtained by heat treatment at corresponding T_x (see Table 1) for 30 min: (a) NTSP04, (b) NTSP06, (c) NTSP08, (d) NTSP10, (e) NTSP12, (f) NTSP14, (g) NTSP16 and (h) NTSP18.

NTSP12 glass-ceramics is homologous to the $K(TiO)PO_4$ (KTP) phase, which present high K^+ ionic conductivity [32,38]. It is worth mentioning that, although the structure of KTP materials is composed of TiO_6 octahedra and PO_4 tetrahedra, which makes it similar to the NASICON structure, its ionic conductivity is anisotropic, probably due to an asymmetry of the TiO_6 octahedra, and it is therefore considered quasi-one-dimensional along the c-axis, remaining in the order of 10^{-6} to 10^{-8} S cm^{-1} at room temperature [32,38].

Some few works in the literature concerning the investigation of the potassium-sodium substitution in the KTP structure, giving rise to the formation of the $K_{1-x}Na_x(TiO)(PO_4)$ system (KNTP) reported the resulting ionic conductivity [29,37,38]. For instance, Loiacono et al. [37] and Glumov et al. [38], have shown that the total conductivity of the KTP system decreases in response to the inclusion of sodium. The aforementioned authors agree that substituting potassium for sodium ions causes the KTP unit cell to shrink because the ionic radius of sodium (1.16 Å) is smaller than that of K^+ (1.51 Å) [33,39]. According to Glumov et al., the decrease in volume presumably hinders the movement of charge carrier ions, thereby increasing the activation energy of 0.34 eV of pure KTP to 0.48 eV of KNTP with sodium. The theoretical results of other authors such as Dahaouid et al. [29] also coincide with those of Glumov et al., in this sense that $NaTiO(PO_4)$ phase is less conductive than KTP. In this regard, and based on the results depicted in Table 3 and Fig. 7-c, the low activation energy (0.31 eV) and high ionic conductivity of the NTSP10 sample at 300 °C (1.7×10^{-2} S cm^{-1}) and at room temperature (1.0×10^{-4} S cm^{-1}) are not consistent with the results obtained by Liacono et al. and Glumov et al. A possible explanation for the high ionic conductivity of the NTSP10 glass-ceramic is that some of the added silica entered the structure to replace phosphorus ions, thus forming a new $Na(TiO)((P,Si)O_4)$ conductive phase, thereby favoring the mobility of Na^+ charge carriers and thus resulting in the decrease in activation energy. The NTSP12

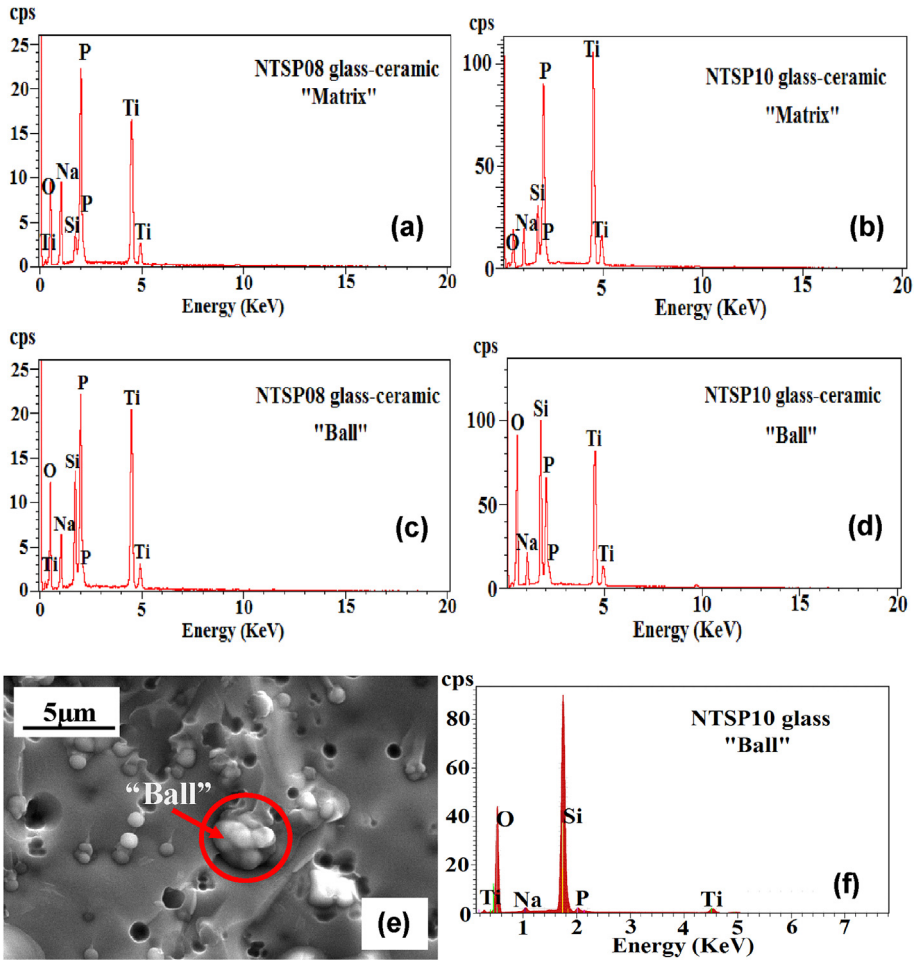

Fig. 6. Chemical composition according to EDS analysis for (a, b) "matrix" and (c, d) "ball" found in NTSP08 and NTSP10 glass-ceramics, respectively. (e) SEM micrograph of fractured surface and (f) EDS analysis for a "ball" of the NTSP10 precursor glass sample.

sample showed lower ionic conductivity than the NTSP10 sample, since the percentage of NTPO phase with silicon ions in place of phosphorus ions, which is presumably responsible for the high ionic conductivity, dropped from 88% ($y = 1.0$) to 57% ($y = 1.2$), according to the Rietveld analysis.

3.5. Synthesis, structure and ionic conductivity of $NaTiO(PO_4)$ (NTPO) glass-ceramics

To check the hypothesis that silicon substitutes phosphorus in the $NaTiO(PO_4)$ structure (as mentioned in Section 3.4), we synthesized the $NaTiO(PO_4)$ (NTPO) compound (without silicon, see Table 4) also via the glass-ceramic route, using the same chemicals and procedure as those described in the experimental section, subsection 2.1, and then, measured its ionic conductivity. The precursor glass was melted at 1250 °C for 15 min. Table 4 describes the T_g and T_x temperatures of the NTPO vitreous material obtained by differential scanning calorimetry.

NTPO glass-ceramic was obtained from the heat treatment of the precursor glass at the crystallization temperature $T_x = 724$ °C, for 30 min. The crystalline material was characterized by X-ray diffraction and then analyzed by Rietveld refinement (Fig. 8-a) for the identification and quantification of the crystalline phases formed after the heat treatment of parent glass.

The X-ray diffraction pattern of the NTPO glass-ceramic material, without silicon, revealed the formation of the $NaTiO(PO_4)$ crystalline phase; some spikes of the NASICON $NaTi_2(PO_4)_3$ as spurious phase were also observed. However, the calculated percentage of the $NaTiO(PO_4)$ crystalline phase is higher (87.8%) than that of the $NaTi_2(PO_4)_3$ phase (12.2%) according to the Rietveld refinement analysis. It is interesting to note that the percentages of $NaTiO(PO)_4$ and NASICON-$NaTi_2(PO_4)_3$ are very similar to those present at the NTSP10 glass-ceramics (see Fig. 4-a).

According to Table 5, the refinement results show that the lattice parameters of the non-NASICON $NaTiO(PO_4)$ cell are smaller in the NTPO sample than in the NTSP10 sample (with silicon), thus indicating a possible substitution of Si^{+4}/P^{+5} at the phosphorus positions within the $NaTiO(PO_4)$ structure. In fact, Si^{+4} (0.26 Å) exhibits a higher ionic radius than the phosphorus ion P^{+5} (0.17 Å). It is worth mentioning that the occupancy factor of Si^{4+} ions could not be resolved by Rietveld refinement, since Si^{+4} and P^{+5} have very similar scattering factors.

The electrical characterization of the NTPO glass-ceramic allowed to determine the ionic conductivity values in different temperatures and thus, the construction of the Arrhenius graph as shown in Fig. 8-b. The values of the activation energy (E_a), total ionic conductivity at room temperature (σ_{RT}) and 300 °C ($\sigma_{300°C}$) and the pre-exponential factor (log σ_0) (Table 6) were estimated from the linear regression of the data in Fig. 8-b.

Table 6 shows that the NTPO sample exhibits an activation energy of 0.40 eV which is higher than the value presented by the NTSP10 sample (0.31 eV). Consequently, the ionic conductivity of

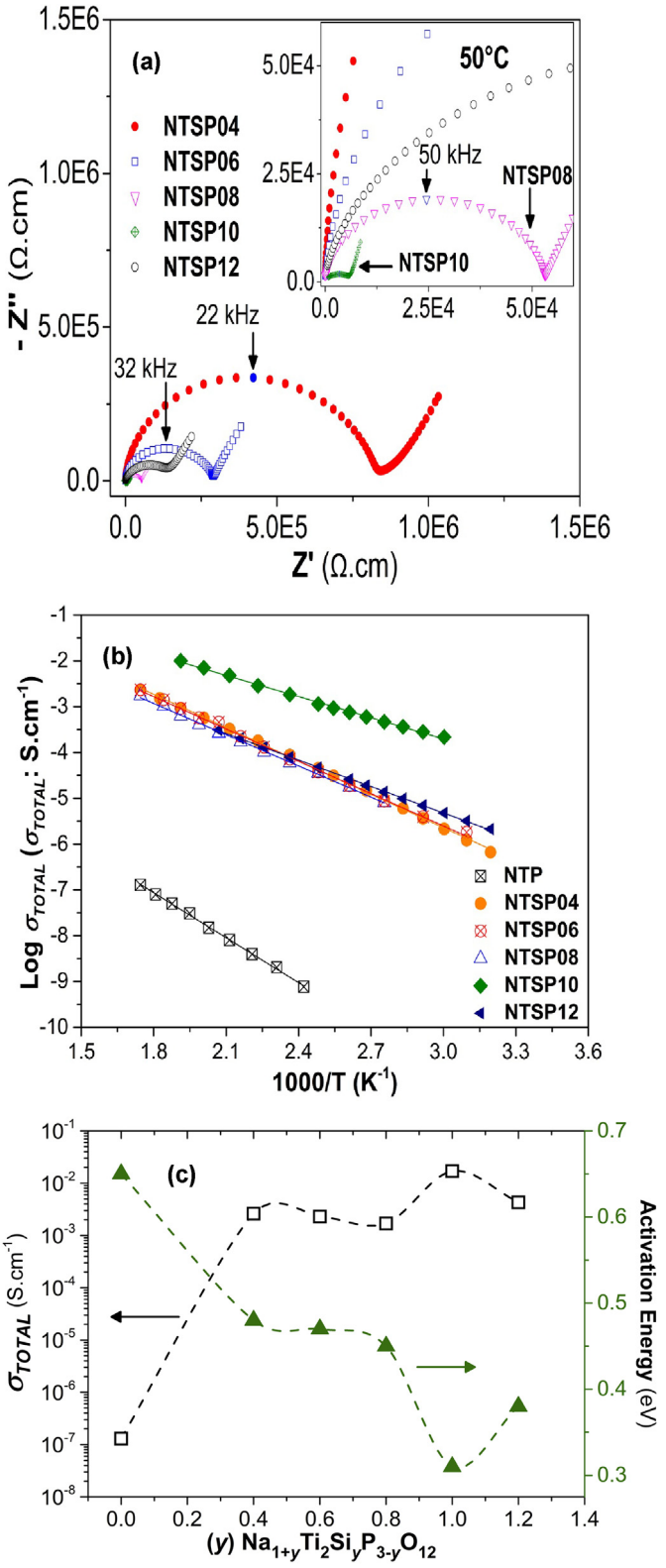

Fig. 7. (a) Complex impedance plot recorded at 50 °C, (b) Arrhenius plot, and (c) variation of σ_{TOTAL} at 300 °C and activation energy as a function of silica content (y) in $Na_{1+y}Ti_2Si_yP_{3-y}O_{12}$ (NTSP) glass-ceramics. The lines represent the linear regression of experimental data in (b) and the dash lines serve to guide the eye in (c).

Table 3
Activation energy (E_a), total conductivity at 300 °C ($\sigma_{300°C}$), and logarithm of pre-exponential factor (log σ_0) of $Na_{1+y}Ti_2Si_yP_{3-y}O_{12}$ (NTSP) glass-ceramics obtained by heat treatment at corresponding T_x (see Table 1) for 30 min.

Sample	E_a (±0.01 eV)[a]	$\sigma_{300°C}$ (S.cm^{-1})	log σ_0 (σ_0: S.cm^{-1})[a]
NTP (without Si)	0.65	1.3×10^{-7}	-1.17 ± 0.08
NTSP04	0.48	2.6×10^{-3}	1.63 ± 0.05
NTSP06	0.47	2.3×10^{-3}	1.44 ± 0.07
NTSP08	0.45	1.7×10^{-3}	1.16 ± 0.04
NTSP10	0.31	1.7×10^{-2}	0.91 ± 0.06
NTSP12	0.38	4.3×10^{-3}	0.45 ± 0.03

[a] Mathematical errors given by linear regression were rounded up to the second decimal case.

Table 4
Nominal composition (mol %) and characteristic temperatures of NTPO precursor glass. T_g = glass transition temperature, T_x = crystallization temperature measured at the onset of the crystallization peak.

Sample	Na_2O	TiO_2	P_2O_5	T_g (°C)	T_x (°C)
	(mol %)			(±2 °C)	(±2 °C)
NTPO	25.0	50.0	25.0	641	724

the NTPO sample is lower than the conductivity of the NTSP10 sample between one and two orders of magnitude according to Fig. 8-b. This result confirms that the possible substitution of silicon by the phosphorus in the $NaTiO(PO_4)$ structure could be favoring the increase of the total ionic conductivity of the compound. To the best of our knowledge, the substitution of P^{5+} by Si^{4+} in the $NaTiO(PO_4)$ or even $KTiO(PO_4)$ (KTP) has never been demonstrated in literature.

4. Conclusions

In the present study, except for the silicon-free composition, precursor glasses were obtained in the whole range of P^{+5}/Si^{+4} substitution in the $Na_{1+y}Ti_2Si_yP_{3-y}O_{12}$ series. Glass-ceramics were obtained in the compositional range of $y = 0.0$ to 2.0. SEM micrographs revealed the presence of silica rich spherical particles in both the glass-ceramics and their parent glasses for $y < 2.0$ compositions. The presence of silica-rich aggregates in some precursor glasses indicates that these glass compositions underwent liquid-liquid phase separation.

The Rietveld analysis revealed that, after heat-treatment of the material at the crystallization onset temperature (T_x), the major phase obtained in the compositions containing up to $y = 0.8$ was the NASICON phase. Conversely, this analysis indicated that the major crystalline phase obtained in the compositions containing $y = 1.0$ and 1.2 was $Na(TiO)(PO_4)$. As for electrical behavior, impedance spectroscopy analysis indicated that the ionic conductivity of samples containing NASICON phase ($y < 1.0$) increased by up to four orders of magnitude in response to the addition of silicon when compared to the samples without silicon, i.e., those containing $NaTi_2(PO_4)_3$. This can be attributed not only to the increase in charge carrier concentration (sodium ions) but also, and mainly, to the expansion of the NASICON-structured unit cell. Interestingly, the higher silicon contents ($y = 1.0$ and 1.2) resulted in glass-ceramics whose main crystalline phase was the non-NASICON $Na(TiO)(PO_4)$. Surprisingly, these glass-ceramics exhibited lower activation energy and higher ionic conductivity than those with NASICON structure. In fact, the $y = 1.0$ sample showed the lowest activation energy (0.31 eV) and the highest total ionic conductivity (1.7×10^{-2} S cm^{-1} at 300 °C and 1.0×10^{-4} S cm^{-1} at room temperature). This high ionic conductivity is attributed to the

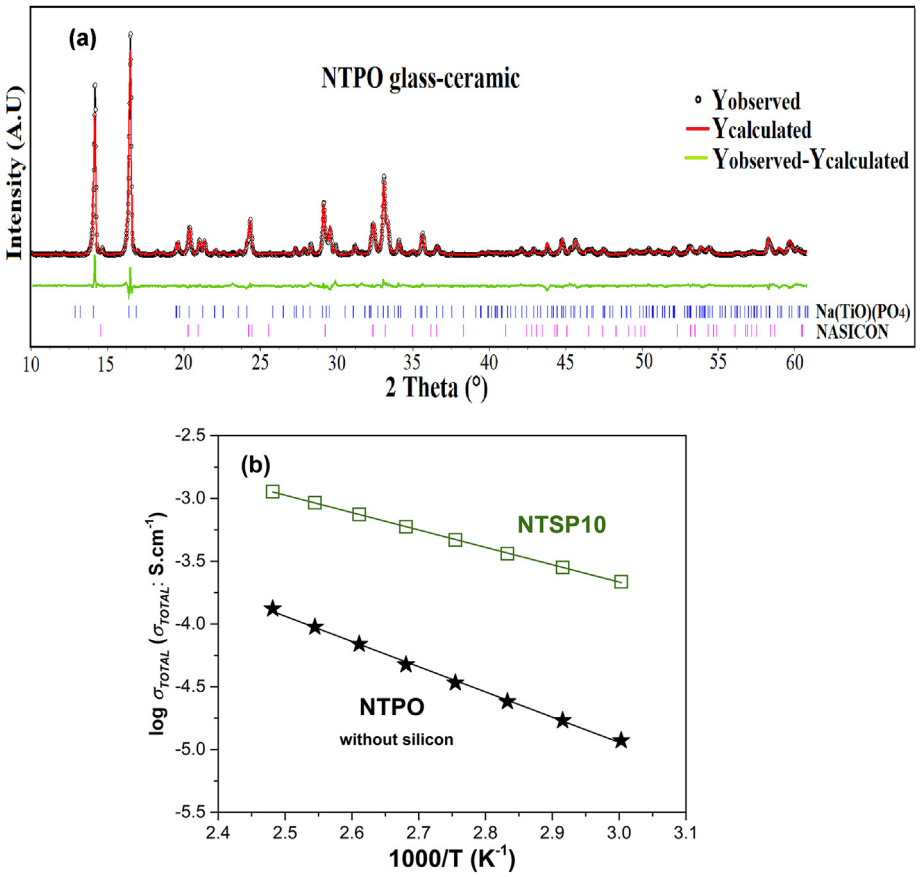

Fig. 8. (a) Rietveld refinement of XRD data of NTPO glass-ceramic and (b) Arrhenius plot of NTSP10 and NTPO samples after heat treatment of their respective precursor glass. The R-factors in the Rietveld analysis were: $R_{wp} = 13.70\%$ and $R_p = 10.18\%$. The lines in (b) represent the linear regression of experimental data.

Table 5
Lattice parameters of the non-NASICON $NaTiO(PO_4)$ structure and *R*-factors (R_{wp} and R_p) from Rietveld analysis of NTPO and NTSP10 glass-ceramics.

Sample	*a* (Å)	*b* (Å)	*c* (Å)	*V* (Å^3)	R_{wp} (%)	R_p (%)
NTPO	8.74	9.10	10.51	837	13.70	10.18
NTSP10	8.75	9.11	10.54	840	10.91	7.97

Table 6
Activation energy (E_a), total conductivity at room temperature (σ_{RT}), total conductivity at 300 °C ($\sigma_{300°C}$), and logarithm of pre-exponential factor (log σ_0) of NTPO glass-ceramic obtained by heat treatment at T_x (see Table 4) for 30 min.

Sample	E_a (±0.01eV)[a]	σ_{RT} (S.cm^{-1})	$\sigma_{300°C}$ (S.cm^{-1})	log σ_0 (σ_0: S.cm^{-1})[a]
NTPO	0.40	2.2×10^{-6}	4.2×10^{-3}	1.15 ± 0.11

[a] Mathematical errors given by linear regression were rounded up to the second decimal case.

substitution of phosphorus ions with silicon ions in the $Na(TiO)(PO_4)$ crystalline phase. This assumption is based on the lattice parameters and electrical characterization of the silicon-free $Na(TiO)PO_4$ compound, which indicated that its ionic conductivity is lower than that of the NTSP10 sample ($y = 1.0$). In conclusion, we can state that we have developed a new sodium conductive glass-ceramic whose conductivity makes it suitable for application as solid electrolyte.

Acknowledgements

The authors gratefully acknowledge the financial support of the Brazilian research funding agencies FAPESP (Fundação de Amparo à Pesquisa do Estado de São Paulo, Process No. 2013–07793, via the CEPID program), CNPq (Conselho Nacional de Desenvolvimento Científico e Tecnológico, under Process No. 168682/2017-6 for JFOM and Process No. 141220/2016-3 for AMNM), and CAPES (Coordenação de Aperfeiçoamento de Pessoal de Nível Superior), Brazil, finance code 001. We are also deeply indebted to C. O. Paiva-Santos for his useful suggestions and help with the Rietveld method.

References

[1] H. Su, S. Jaffer, H. Yu, Transition metal oxides for sodium-ion batteries, Energy Stor. Mater. 5 (2016) 116–131, https://doi.org/10.1016/j.ensm.2016.06.005.
[2] B.L. Ellis, L.F. Nazar, Sodium and sodium-ion energy storage batteries, Curr. Opin. Solid State Mater. Sci. 16 (2012) 168–177, https://doi.org/10.1016/j.cossms.2012.04.002.
[3] M.I. Jamesh, A.S. Prakash, Advancement of technology towards developing Na-ion batteries, J. Power Sources 378 (2018) 268–300, https://doi.org/10.1016/j.jpowsour.2017.12.053.
[4] K.B. Hueso, M. Armand, T. Rojo, High temperature sodium batteries: status, challenges and future trends, Energy Environ. Sci. 6 (2013) 734–749, https://doi.org/10.1039/c3ee24086j.
[5] Y. Wang, R. Chen, T. Chen, H. Lv, G. Zhu, L. Ma, C. Wang, Z. Jin, J. Liu, Emerging non-lithium ion batteries, Energy Stor. Mater. 4 (2016) 103–129, https://doi.org/10.1016/j.ensm.2016.04.001.
[6] Y. Fang, J. Zhang, L. Xiao, X. Ai, Y. Cao, H. Yang, Phosphate framework electrode materials for sodium ion batteries, Adv. Sci. 4 (2017), https://doi.org/10.1002/advs.201600392.
[7] H. Kang, Y. Liu, K. Cao, Y. Zhao, L. Jiao, Y. Wang, H. Yuan, Update on anode materials for Na-ion batteries, J. Mater. Chem. A. 3 (2015) 17899–17913, https://doi.org/10.1039/C5TA03181H.

[8] H. Bradtmüller, A.M. Nieto-Muñoz, J.F. Ortiz-Mosquera, A.C.M. Rodrigues, H. Eckert, Glass-to-crystal transition in the NASICON glass-ceramic system $Na_{1+x}Al_xM_{2-x}(PO_4)_3$ (M=Ge, Ti), J. Non-Cryst. Solids 489 (2018) 91–101, https://doi.org/10.1016/j.jnoncrysol.2017.10.057.
[9] M. Guin, F. Tietz, Survey of the transport properties of sodium superionic conductor materials for use in sodium batteries, J. Power Sources 273 (2015) 1056–1064, https://doi.org/10.1016/j.jpowsour.2014.09.137.
[10] J. Thomas, in: PeterG. Bruce (Ed.), Solid State Electrochemistry, vol. XVI, Cambridge University Press, Cambridge, 1995, p. 344, https://doi.org/10.1002/adma.19960080417. ISBN 0-521-40007-4, Adv. Mater. 8 (1996) 360–360.
[11] R.M. Dell, Batteries: fifty years of materials development, Solid State Ion. 134 (2000) 139–158, https://doi.org/10.1016/S0167-2738(00)00722-0.
[12] F. Lalère, J.B. Leriche, M. Courty, S. Boulineau, V. Viallet, C. Masquelier, V. Seznec, An all-solid state NASICON sodium battery operating at 200°C, J. Power Sources 247 (2014) 975–980, https://doi.org/10.1016/j.jpowsour.2013.09.051.
[13] W. Zhou, Y. Li, S. Xin, J.B. Goodenough, Rechargeable sodium all-solid-state battery, ACS Cent. Sci. 3 (2017) 52–57, https://doi.org/10.1021/acscentsci.6b00321.
[14] J.L. Narváez-Semanate, A.C.M. Rodrigues, Microstructure and ionic conductivity of $Li_{1+x}Al_xTi_{2-x}(PO_4)_3$ NASICON glass-ceramics, Solid State Ion. 181 (2010) 1197–1204, https://doi.org/10.1016/j.ssi.2010.05.010.
[15] J.F. Ortiz-Mosquera, A.M. Nieto-Muñoz, A.C.M. Rodrigues, Precursor glass stability, microstructure and ionic conductivity of glass-ceramics from the $Na_{1+x}Al_xGe_{2-x}(PO_4)_3$ NASICON series, J. Non-Cryst. Solids 513 (2019) 36–43, https://doi.org/10.1016/j.jnoncrysol.2019.03.008.
[16] N. Anantharamulu, K.K. Rao, G. Rambabu, B.V. Kumar, V. Radha, M. Vithal, A Wide-Ranging Review on Nasicon Type Materials, 2011, pp. 2821–2837, https://doi.org/10.1007/s10853-011-5302-5.
[17] Z. Jian, Y.S. Hu, X. Ji, W. Chen, NASICON-structured materials for energy storage, Adv. Mater. 29 (2017), https://doi.org/10.1002/adma.201601925.
[18] B.E. Francisco, C.R. Stoldt, J.-C. M'Peko, Lithium-ion trapping from local structural distortions in NASICON electrolytes, Chem. Mater. (2014) 4741–4749, https://doi.org/10.1021/cm5013872.
[19] M. Barré, M.P. Crosnier-Lopez, F. Le Berre, E. Suard, J.L. Fourquet, Synthesis and structural study of a new NASICON-type solid solution: $Li_{1-x}La_{x/3}Zr_2(PO_4)_3$, J. Solid State Chem. 180 (2007) 1011–1019, https://doi.org/10.1016/j.jssc.2006.12.032.
[20] R.B. Nuernberg, A.C.M. Rodrigues, A new NASICON lithium ion-conducting glass-ceramic of the $Li_{1+x}Cr_x(Ge_yTi_{1-y})_{2-x}(PO_4)_3$ system, Solid State Ion. 301 (2017) 1–9, https://doi.org/10.1016/j.ssi.2017.01.004.
[21] A. Tsuji, H. Takahashi, T. Oi, Preparation of ion exchangers in the hydrogen form from $M_{1+x}Ti_2P_{3-x}Si_xO_{12}$(M = Li, Na) crystals and glass-ceramics and their characterization, J. Mater. Chem. 13 (2003) 542–549, https://doi.org/10.1039/b207611j.
[22] A. Kishioka, Y. Miyazawa, K. Itatani, F.S. Howell, M. Kinoshita, Preparation and properties of phosphate glasses and glass-ceramics containing large amounts of titanium (IV), J. Ceram. Soc. Jpn. 102 (1994) 155–159, https://doi.org/10.2109/jcersj.102.155.
[23] J. Fu, Superionic conductivity of glass-ceramics in the system Li 2 O- Al 2 O 3 -TiO 2 -P 2 O 5, Solid State Ion. 96 (1997) 195–200, https://doi.org/10.1016/S0167-2738(97)00018-0.
[24] Oxford Cryosystems, Crystallographica search-match, J. Appl. Crystallogr. 32 (1999) 379–380, https://doi.org/10.1107/s0021889899004124.
[25] A.A. Coelho, J. Evans, I. Evans, A. Kern, S. Parsons, The TOPAS symbolic computation system, Powder Diffr. 26 (2011) S22–S25, https://doi.org/10.1154/1.3661087.
[26] A. Belsky, M. Hellenbrandt, V.L. Karen, P. Luksch, New developments in the Inorganic Crystal Structure Database (ICSD): accessibility in support of materials research and design, Acta Crystallogr. Sect. B Struct. Sci. 58 (2002) 364–369, https://doi.org/10.1107/S0108768102006948.
[27] V.M. Fokin, R.M.C.V. Reis, A.S. Abyzov, C.R. Chinaglia, E.D. Zanotto, Non-stoichiometric crystallization of lithium metasilicate–calcium metasilicate glasses. Part 1 — crystal nucleation and growth rates, J. Non-Cryst. Solids 362 (2013) 56–64, https://doi.org/10.1016/j.jnoncrysol.2012.11.020.
[28] L.S. Gallo, T. De Marchi Mosca, B.H. Teider, I. Polyakova, A.C.M. Rodrigues, E.D. Zanotto, V.M. Fokin, Effects of lithium oxide on the crystallization kinetics of $Na_2O{\cdot}2CaO{\cdot}3SiO_2$ glass, J. Non-Cryst. Solids 408 (2015) 102–114, https://doi.org/10.1016/j.jnoncrysol.2014.10.018.
[29] S. Dahaoui, N.K. Hansen, J. Protas, H.-G. Krane, K. Fischer, G. Marnier, Electric properties of $KTiOPO_4$ and $NaTiOPO_4$ from temperature-dependent X-ray diffraction, J. Appl. Crystallogr. 32 (1999) 1–10, https://doi.org/10.1107/S002188989800497X.
[30] P.I. Tordjman, E. Masse, J.C. Guitel, Structure cristalline du monophosphate $KTiPO_5$, Z. Krist. 139 (1974) 103–115, https://doi.org/10.1524/zkri.1974.139.1-2.103.
[31] B.-C. Choi, B.K. Moon, H.-J. Seo, J.-H. Park, C.-S. Kim, Impedance spectroscopy of $KTiOPO_4$ single crystal in the temperature range -100 to 100°C, Appl. Phys. Mater. Sci. Process 78 (2004) 745–748, https://doi.org/10.1007/s00339-002-2026-z.
[32] P.A. Morris, A. Ferretti, J.D. Bierlein, G.M. Loiacono, Reduction of the ionic conductivity of flux grown KTiOPO 4 crystals, J. Cryst. Growth 109 (1991) 367–375, https://doi.org/10.1016/0022-0248(91)90205-J.
[33] R.D. Shannon, Revised effective ionic radii and systematic studies of interatomic distances in halides and chalcogenides, Acta Crystallogr. A 32 (1976) 751–767, https://doi.org/10.1107/S0567739476001551.
[34] K. Shimazu, Y. Yamamoto, Y. Saito, O. Nakamura, Electrical conductivity and Ti4+ ion substitution range in NASICON system, Solid State Ion. 79 (1995) 106–110, https://doi.org/10.1016/0167-2738(95)00038-8.
[35] P. Yadav, M.C. Bhatnagar, Preparation, structure and conductivity of Sn modified NASICON material, J. Electroceram. 30 (2013) 145–151, https://doi.org/10.1007/s10832-012-9776-6.
[36] J.M. Oliveira, R.N. Correia, M.H.V. Fernandes, formation of convoluted silica precipitates during amorphous phase separation in the $Ca_3(PO_4)_2$-SiO_2-MgO system, J. Am. Ceram. Soc. 83 (2004) 1296–1298, https://doi.org/10.1111/j.1151-2916.2000.tb01374.x.
[37] G.M. Loiacono, D.N. Loiacono, R.A. Stolzenberger, Growth and properties of crystals in the system $KTiOPO_4$-$NaTiOPO_4$, J. Cryst. Growth 144 (1994) 223–228, https://doi.org/10.1016/0022-0248(94)90460-X.
[38] O.V. Glumov, V.A. Bodnar, N.A. Mel'nikova, V.E. Yakobson, I.V. Murin, Electrical conductivity of potassium titanyl phosphate KTiOPO4 pure crystals and those doped with Na^+, Rb^+, and F^- ions, Russ. J. Electrochem. 53 (2017) 846–851, https://doi.org/10.1134/S1023193517080055.
[39] G.M. Loiacono, R.A. Stolzenberger, D.N. Loiacono, Modified $KTiOPO_4$ crystals for noncritical phase matching applications, Appl. Phys. Lett. 64 (1994) 16–18, https://doi.org/10.1063/1.111959.